

W Production and the Search for Events with an Isolated High-Energy Lepton and Missing Transverse Momentum at HERA

ZEUS Collaboration

Abstract

A search for the leptonic decays of W bosons produced in the reaction $e^+p \rightarrow e^+W^\pm X$ at a centre-of-mass energy of 300 GeV has been performed with the ZEUS detector at HERA using an integrated luminosity of 47.7 pb^{-1} . Three events consistent with $W \rightarrow e\nu$ decay are found, giving a cross section estimate of $0.9_{-0.7}^{+1.0} \pm 0.2 \text{ pb}$, in good agreement with the Standard Model prediction. The corresponding 95% C.L. upper limit on the cross section is 3.3 pb. A search for the decay $W \rightarrow \mu\nu$ has a smaller selection efficiency and yields no candidate events. Limits on the cross section for W production with large hadronic transverse momentum have been obtained. A search for high-transverse-momentum isolated tracks in events with large missing transverse momentum yields results in good agreement with Standard Model expectations, in contrast to a recent report by the H1 collaboration of the observation of an excess of such events.

The ZEUS Collaboration

J. Breitweg, S. Chekanov, M. Derrick, D. Krakauer, S. Magill, B. Musgrave, A. Pellegrino,
J. Repond, R. Stanek, R. Yoshida

Argonne National Laboratory, Argonne, IL, USA ^p

M.C.K. Mattingly

Andrews University, Berrien Springs, MI, USA

G. Abbiendi, F. Anselmo, P. Antonioli, G. Bari, M. Basile, L. Bellagamba, D. Boscherini¹,
A. Bruni, G. Bruni, G. Cara Romeo, G. Castellini², L. Cifarelli³, F. Cindolo, A. Contin,
N. Coppola, M. Corradi, S. De Pasquale, P. Giusti, G. Iacobucci⁴, G. Laurenti, G. Levi,
A. Margotti, T. Massam, R. Nania, F. Palmonari, A. Pesci, A. Polini, G. Sartorelli,
Y. Zamora Garcia⁵, A. Zichichi

University and INFN Bologna, Bologna, Italy ^f

C. Amelung, A. Bornheim, I. Brock, K. Coböken, J. Crittenden, R. Deffner, M. Eckert⁶,
H. Hartmann, K. Heinloth, E. Hilger, H.-P. Jakob, A. Kappes, U.F. Katz, R. Kerger,
E. Paul, J. Rautenberg⁷, H. Schnurbusch, A. Stifutkin, J. Tandler, A. Weber, H. Wieber
Physikalisches Institut der Universität Bonn, Bonn, Germany ^c

D.S. Bailey, O. Barret, W.N. Cottingham, B. Foster⁸, G.P. Heath, H.F. Heath,
J.D. McFall, D. Piccioni, J. Scott, R.J. Tapper

H.H. Wills Physics Laboratory, University of Bristol, Bristol, U.K. ^{o r}

M. Capua, A. Mastroberardino, M. Schioppa, G. Susinno

Calabria University, Physics Dept. and INFN, Cosenza, Italy ^f

H.Y. Jeoung, J.Y. Kim, J.H. Lee, I.T. Lim, K.J. Ma, M.Y. Pac⁹

Chonnam National University, Kwangju, Korea ^h

A. Caldwell, N. Cartiglia, Z. Jing, W. Liu, B. Mellado, J.A. Parsons, S. Ritz¹⁰, R. Sacchi,
S. Sampson, F. Sciulli, Q. Zhu¹¹

Columbia University, Nevis Labs., Irvington on Hudson, N.Y., USA ^q

J. Chwastowski, A. Eskreys, J. Figiel, K. Klimek, K. Olkiewicz, M.B. Przybycień, P. Stopa,
L. Zawiejski

Inst. of Nuclear Physics, Cracow, Poland ^j

L. Adamczyk¹², B. Bednarek, K. Jeleń, D. Kisiielewska, A.M. Kowal, T. Kowalski,
M. Przybycień, E. Rulikowska-Zarebska, L. Suszycki, J. Zając

*Faculty of Physics and Nuclear Techniques, Academy of Mining and Metallurgy, Cracow,
Poland ^j*

Z. Duliński, A. Kotański

Jagellonian Univ., Dept. of Physics, Cracow, Poland ^k

L.A.T. Bauerdick, U. Behrens, J.K. Bienlein, C. Burgard, K. Desler, G. Drews, A. Fox-Murphy, U. Fricke, F. Goebel, P. Göttlicher, R. Graciani, T. Haas, W. Hain, G.F. Hartner, D. Hasell¹³, K. Hebbel, K.F. Johnson¹⁴, M. Kasemann¹⁵, W. Koch, U. Kötz, H. Kowalski, L. Lindemann, B. Löhr, M. Martínez, J. Milewski¹⁶, M. Milite, T. Monteiro¹⁷, M. Moritz, D. Notz, F. Pelucchi, K. Piotrkowski, M. Rohde, P.R.B. Saull, A.A. Savin, U. Schneekloth, O. Schwarzer¹⁸, F. Selonke, M. Sievers, S. Stonjek, E. Tassi, G. Wolf, U. Wollmer, C. Youngman, W. Zeuner
Deutsches Elektronen-Synchrotron DESY, Hamburg, Germany

B.D. Burow¹⁹, C. Coldewey, H.J. Grabosch, A. Lopez-Duran Viani, A. Meyer, K. Mönig, S. Schlenstedt, P.B. Straub
DESY Zeuthen, Zeuthen, Germany

G. Barbagli, E. Gallo, P. Pelfer
University and INFN, Florence, Italy^f

G. Maccarrone, L. Votano
INFN, Laboratori Nazionali di Frascati, Frascati, Italy^f

A. Bamberger, S. Eisenhardt²⁰, P. Markun, H. Raach, S. Wölffe
Fakultät für Physik der Universität Freiburg i.Br., Freiburg i.Br., Germany^c

N.H. Brook²¹, P.J. Bussey, A.T. Doyle, S.W. Lee, N. Macdonald, G.J. McCance, D.H. Saxon, L.E. Sinclair, I.O. Skillicorn, E. Strickland, R. Waugh
Dept. of Physics and Astronomy, University of Glasgow, Glasgow, U.K.^o

I. Bohnet, N. Gendner, U. Holm, A. Meyer-Larsen, H. Salehi, K. Wick
Hamburg University, I. Institute of Exp. Physics, Hamburg, Germany^c

A. Garfagnini, I. Gialas²², L.K. Gladilin²³, D. Kçira²⁴, R. Klanner, E. Lohrmann, G. Poelz, F. Zetsche
Hamburg University, II. Institute of Exp. Physics, Hamburg, Germany^c

T.C. Bacon, J.E. Cole, G. Howell, L. Lamberti²⁵, K.R. Long, D.B. Miller, A. Priniias²⁶, J.K. Sedgbeer, D. Sideris, A.D. Tapper, R. Walker
Imperial College London, High Energy Nuclear Physics Group, London, U.K.^o

U. Mallik, S.M. Wang
University of Iowa, Physics and Astronomy Dept., Iowa City, USA^p

P. Cloth, D. Filges
Forschungszentrum Jülich, Institut für Kernphysik, Jülich, Germany

T. Ishii, M. Kuze, I. Suzuki²⁷, K. Tokushuku²⁸, S. Yamada, K. Yamauchi, Y. Yamazaki
Institute of Particle and Nuclear Studies, KEK, Tsukuba, Japan^{g s}

S.H. Ahn, S.H. An, S.J. Hong, S.B. Lee, S.W. Nam²⁹, S.K. Park
Korea University, Seoul, Korea^h

H. Lim, I.H. Park, D. Son
Kyungpook National University, Taegu, Korea^h

F. Barreiro, J.P. Fernández, G. García, C. Glasman³⁰, J.M. Hernández³¹, L. Labarga, J. del Peso, J. Puga, I. Redondo³², J. Terrón
*Univer. Autónoma Madrid, Depto de Física Teórica, Madrid, Spain*ⁿ

F. Corriveau, D.S. Hanna, J. Hartmann³³, W.N. Murray³⁴, A. Ochs, S. Padhi, M. Riveline, D.G. Stairs, M. St-Laurent, M. Wing
McGill University, Dept. of Physics, Montréal, Québec, Canada^{a, b}

T. Tsurugai
Meiji Gakuin University, Faculty of General Education, Yokohama, Japan

V. Bashkirov³⁵, B.A. Dolgoshein
Moscow Engineering Physics Institute, Moscow, Russia^l

G.L. Bashindzhagyan, P.F. Ermolov, Yu.A. Golubkov, L.A. Khein, N.A. Korotkova, I.A. Korzhavina, V.A. Kuzmin, O.Yu. Lukina, A.S. Proskuryakov, L.M. Shcheglova³⁶, A.N. Solomin³⁶, S.A. Zotkin
Moscow State University, Institute of Nuclear Physics, Moscow, Russia^m

C. Bokel, M. Botje, N. Brümmer, J. Engelen, E. Koffeman, P. Kooijman, A. van Sighem, H. Tiecke, N. Tuning, J.J. Velthuis, W. Verkerke, J. Vosseveld, L. Wiggers, E. de Wolf
*NIKHEF and University of Amsterdam, Amsterdam, Netherlands*ⁱ

D. Acosta³⁷, B. Bylsma, L.S. Durkin, J. Gilmore, C.M. Ginsburg, C.L. Kim, T.Y. Ling, P. Nylander
Ohio State University, Physics Department, Columbus, Ohio, USA^p

H.E. Blaikley, S. Boogert, R.J. Cashmore¹⁷, A.M. Cooper-Sarkar, R.C.E. Devenish, J.K. Edmonds, J. Große-Knetter³⁸, N. Harnew, T. Matsushita, V.A. Noyes³⁹, A. Quadt¹⁷, O. Ruske, M.R. Sutton, R. Walczak, D.S. Waters
Department of Physics, University of Oxford, Oxford, U.K.^{o s}

A. Bertolin, R. Brugnera, R. Carlin, F. Dal Corso, S. Dondana, U. Dosselli, S. Dusini, S. Limentani, M. Morandin, M. Posocco, L. Stanco, R. Stroili, C. Voci
Dipartimento di Fisica dell' Università and INFN, Padova, Italy^f

L. Iannotti⁴⁰, B.Y. Oh, J.R. Okrasinski, W.S. Toothacker, J.J. Whitmore
Pennsylvania State University, Dept. of Physics, University Park, PA, USA^q

Y. Iga
Polytechnic University, Sagamihara, Japan^g

G. D'Agostini, G. Marini, A. Nigro, M. Raso
Dipartimento di Fisica, Univ. 'La Sapienza' and INFN, Rome, Italy^f

C. Cormack, J.C. Hart, N.A. McCubbin, T.P. Shah
Rutherford Appleton Laboratory, Chilton, Didcot, Oxon, U.K.^o

D. Epperson, C. Heusch, H.F.-W. Sadrozinski, A. Seiden, R. Wichmann, D.C. Williams
University of California, Santa Cruz, CA, USA^p

N. Pavel

Fachbereich Physik der Universität-Gesamthochschule Siegen, Germany^c

H. Abramowicz⁴¹, S. Dagan⁴², S. Kananov⁴², A. Kreisel, A. Levy⁴²

Raymond and Beverly Sackler Faculty of Exact Sciences, School of Physics, Tel-Aviv University, Tel-Aviv, Israel^e

T. Abe, T. Fusayasu, M. Inuzuka, K. Nagano, K. Umemori, T. Yamashita

Department of Physics, University of Tokyo, Tokyo, Japan^g

R. Hamatsu, T. Hirose, K. Homma⁴³, S. Kitamura⁴⁴, T. Nishimura

Tokyo Metropolitan University, Dept. of Physics, Tokyo, Japan^g

M. Arneodo⁴⁵, R. Cirio, M. Costa, M.I. Ferrero, S. Maselli, V. Monaco, C. Peroni,

M.C. Petrucci, M. Ruspa, A. Solano, A. Staiano

Università di Torino, Dipartimento di Fisica Sperimentale and INFN, Torino, Italy^f

M. Dardo

II Faculty of Sciences, Torino University and INFN - Alessandria, Italy^f

D.C. Bailey, C.-P. Fagerstroem, R. Galea, T. Koop, G.M. Levman, J.F. Martin, R.S. Orr,
S. Polenz, A. Sabetfakhri, D. Simmons

University of Toronto, Dept. of Physics, Toronto, Ont., Canada^a

J.M. Butterworth, C.D. Catterall, M.E. Hayes, E.A. Heaphy, T.W. Jones, J.B. Lane,
B.J. West

University College London, Physics and Astronomy Dept., London, U.K.^o

J. Ciborowski, R. Ciesielski, G. Grzelak, R.J. Nowak, J.M. Pawlak, R. Pawlak, B. Smalska,
T. Tymieniecka, A.K. Wróblewski, J.A. Zakrzewski, A.F. Żarnecki

Warsaw University, Institute of Experimental Physics, Warsaw, Poland^j

M. Adamus, T. Gadaj

Institute for Nuclear Studies, Warsaw, Poland^j

O. Deppe, Y. Eisenberg⁴², D. Hochman, U. Karshon⁴²

Weizmann Institute, Department of Particle Physics, Rehovot, Israel^d

W.F. Badgett, D. Chapin, R. Cross, C. Foudas, S. Mattingly, D.D. Reeder, W.H. Smith,
A. Vaiciulis⁴⁶, T. Wildschek, M. Wodarczyk

University of Wisconsin, Dept. of Physics, Madison, WI, USA^p

A. Deshpande, S. Dhawan, V.W. Hughes

Yale University, Department of Physics, New Haven, CT, USA^p

S. Bhadra, W.R. Frisken, R. Hall-Wilton, M. Khakzad, S. Menary, W.B. Schmidke

York University, Dept. of Physics, Toronto, Ont., Canada^a

¹ now visiting scientist at DESY
² also at IROE Florence, Italy
³ now at Univ. of Salerno and INFN Napoli, Italy
⁴ also at DESY
⁵ supported by Worldlab, Lausanne, Switzerland
⁶ now at BSG Systemplanung AG, 53757 St. Augustin
⁷ drafted to the German military service
⁸ also at University of Hamburg, Alexander von Humboldt Research Award
⁹ now at Dongshin University, Naju, Korea
¹⁰ now at NASA Goddard Space Flight Center, Greenbelt, MD 20771, USA
¹¹ now at Greenway Trading LLC
¹² supported by the Polish State Committee for Scientific Research, grant No. 2P03B14912
¹³ now at Massachusetts Institute of Technology, Cambridge, MA, USA
¹⁴ visitor from Florida State University
¹⁵ now at Fermilab, Batavia, IL, USA
¹⁶ now at ATM, Warsaw, Poland
¹⁷ now at CERN
¹⁸ now at ESG, Munich
¹⁹ now an independent researcher in computing
²⁰ now at University of Edinburgh, Edinburgh, U.K.
²¹ PPARC Advanced fellow
²² visitor of Univ. of Crete, Greece, partially supported by DAAD, Bonn - Kz. A/98/16764
²³ on leave from MSU, supported by the GIF, contract I-0444-176.07/95
²⁴ supported by DAAD, Bonn - Kz. A/98/12712
²⁵ supported by an EC fellowship
²⁶ PPARC Post-doctoral fellow
²⁷ now at Osaka Univ., Osaka, Japan
²⁸ also at University of Tokyo
²⁹ now at Wayne State University, Detroit
³⁰ supported by an EC fellowship number ERBFMBICT 972523
³¹ now at HERA-B/DESY supported by an EC fellowship No.ERBFMBICT 982981
³² supported by the Comunidad Autonoma de Madrid
³³ now at debis Systemhaus, Bonn, Germany
³⁴ now a self-employed consultant
³⁵ now at Loma Linda University, Loma Linda, CA, USA
³⁶ partially supported by the Foundation for German-Russian Collaboration DFG-RFBR
(grant no. 436 RUS 113/248/3 and no. 436 RUS 113/248/2)
³⁷ now at University of Florida, Gainesville, FL, USA
³⁸ supported by the Feodor Lynen Program of the Alexander von Humboldt foundation
³⁹ now with Physics World, Dirac House, Bristol, U.K.
⁴⁰ partly supported by Tel Aviv University
⁴¹ an Alexander von Humboldt Fellow at University of Hamburg
⁴² supported by a MINERVA Fellowship
⁴³ now at ICEPP, Univ. of Tokyo, Tokyo, Japan
⁴⁴ present address: Tokyo Metropolitan University of Health Sciences, Tokyo 116-8551,

Japan

⁴⁵ now also at Università del Piemonte Orientale, I-28100 Novara, Italy, and Alexander von Humboldt fellow at the University of Hamburg

⁴⁶ now at University of Rochester, Rochester, NY, USA

- ^a supported by the Natural Sciences and Engineering Research Council of Canada (NSERC)
- ^b supported by the FCAR of Québec, Canada
- ^c supported by the German Federal Ministry for Education and Science, Research and Technology (BMBF), under contract numbers 057BN19P, 057FR19P, 057HH19P, 057HH29P, 057SI75I
- ^d supported by the MINERVA Gesellschaft für Forschung GmbH, the German Israeli Foundation, and by the Israel Ministry of Science
- ^e supported by the German-Israeli Foundation, the Israel Science Foundation, the U.S.-Israel Binational Science Foundation, and by the Israel Ministry of Science
- ^f supported by the Italian National Institute for Nuclear Physics (INFN)
- ^g supported by the Japanese Ministry of Education, Science and Culture (the Monbusho) and its grants for Scientific Research
- ^h supported by the Korean Ministry of Education and Korea Science and Engineering Foundation
- ⁱ supported by the Netherlands Foundation for Research on Matter (FOM)
- ^j supported by the Polish State Committee for Scientific Research, grant No. 115/E-343/SPUB/P03/154/98, 2P03B03216, 2P03B04616, 2P03B10412, 2P03B05315, 2P03B03517, and by the German Federal Ministry of Education and Science, Research and Technology (BMBF)
- ^k supported by the Polish State Committee for Scientific Research (grant No. 2P03B08614 and 2P03B06116)
- ^l partially supported by the German Federal Ministry for Education and Science, Research and Technology (BMBF)
- ^m supported by the Fund for Fundamental Research of Russian Ministry for Science and Education and by the German Federal Ministry for Education and Science, Research and Technology (BMBF)
- ⁿ supported by the Spanish Ministry of Education and Science through funds provided by CICYT
- ^o supported by the Particle Physics and Astronomy Research Council
- ^p supported by the US Department of Energy
- ^q supported by the US National Science Foundation
- ^r partially supported by the British Council, ARC Project 0867.00
- ^s partially supported by the British Council, Collaborative Research Project, TOK/880/11/15

1 Introduction

This paper reports the results of an investigation into the production of W bosons in positron-proton collisions at HERA. The collider operated from 1994 to 1997 with positron and proton beam energies of 27.5 and 820 GeV respectively, resulting in a centre-of-mass energy of 300 GeV. During this period the ZEUS detector collected data corresponding to an integrated luminosity of 47.7 pb^{-1} .

The Standard Model calculation of the cross section for the production of W bosons via the reaction $e^+p \rightarrow e^+W^\pm X$ yields a value of roughly 1 pb [1, 2, 3]. The W -production cross section is sensitive to the couplings at the $WW\gamma$ vertex, particularly at large hadronic transverse momentum (“hadronic P_T ”). A measurement of the cross section can therefore provide limits on anomalous $WW\gamma$ couplings. In addition, the measurement gives a useful constraint on the W -production background to a variety of searches for non-Standard-Model physics at HERA.

The search for signals for W production in both the electron¹ and muon decay channels was performed by selecting events with large missing transverse momentum (“missing P_T ”) which also contain isolated leptons with high transverse momentum (“high P_T ”). The result of the search in each decay channel is consistent with Standard Model expectations. The integrated luminosity and the signal-to-background ratio in the electron channel search are sufficient to allow a first estimate of the cross section for W production in electron-proton interactions. The searches in the two decay channels are combined at large hadronic P_T in order to obtain cross-section limits in this region, and limits on the couplings at the $WW\gamma$ triple-gauge-boson vertex are calculated.

The H1 collaboration has recently reported the observation of six events containing isolated high-energy leptons and missing transverse momentum [4]. The number of muon events is significantly larger than the Standard Model expectation, to which W production forms the major contribution. A search for such events with the ZEUS detector, using similar cuts and with a similar sensitivity to that of the H1 analysis, yields results in good agreement with the Standard Model.

In Section 2 of this article, the W -production signal and its simulation are discussed in more detail. Background processes are treated in Section 3. Section 4 describes the ZEUS detector. Details of the event reconstruction and pre-selection are given in Section 5. The results of the analysis in the electron and muon channels are presented in Sections 6 and 7, respectively. Section 8 presents upper limits on the cross section for W production at large hadronic P_T , while Section 9 presents the ZEUS analysis of events containing an isolated high-energy charged particle in addition to large missing transverse momentum. The results are summarised in Section 10.

¹The term electron is used to refer to both electrons and positrons.

2 W Production at HERA

The dominant W -production process in e^+p collisions at HERA is the reaction

$$e^+p \rightarrow e^+W^\pm X, \quad (1)$$

in which the scattered beam electron emerges at small angles with respect to the lepton beam direction and is generally not found in the central detector. The observed event topology therefore consists of the hadronic final state X , which typically carries small transverse momentum, and the W decay products at comparatively large laboratory angles.

2.1 Cross-Section Calculation

The leading-order diagrams for reaction (1) are shown in Fig. 1. Diagrams (a) and (b) correspond to W radiation from the incoming and scattered quark, respectively. Diagrams (f) and (g), in which the W couples to the incoming or scattered lepton line, are suppressed by a second heavy propagator. Diagram (c) contains the $WW\gamma$ triple-gauge-boson coupling. Diagrams (d) and (e), required to preserve gauge invariance, contain off-shell W 's which give rise primarily to low- P_T charged leptons and lepton-neutrino invariant masses far from the W mass.

The contributions of the different diagrams are calculated with the Monte Carlo based program EPVEC [2]. The fermion u -channel pole of diagram (a) is regularised by splitting the phase space into two regions :

$$\sigma = \sigma(|u| > u_{cut}) + \int^{u_{cut}} \frac{d\sigma}{d|u|} d|u|$$

where $u = (p_q - p_W)^2$ and p_q, p_W are the four momenta of the incoming quark and final state W boson, respectively. The first term is calculated using helicity amplitudes for the process $e^+q \rightarrow e^+Wq', W \rightarrow f\bar{f}'$. The cross section for small values of $|u|$ is calculated by folding the cross section for $q\bar{q}' \rightarrow W \rightarrow f\bar{f}'$ with the parton densities in the proton and the effective parton densities for the resolved photon emitted by the incoming electron. The resulting total cross section for reaction (1) varies little with u_{cut} , chosen here to be 25 GeV^2 .

Using the MRS(G) [5] set of parton densities in the proton evaluated at a scale M_W^2 and the GRVG-LO [6] set of parton densities in the photon evaluated at a scale $p_W^2/10$, the cross sections are 0.52 pb for W^+ and 0.42 pb for W^- production via reaction (1), giving a total of 0.95 pb .

The cross section for the process $e^+p \rightarrow \bar{\nu}W^+X$, also calculated using EPVEC, is only about 5% of that for reaction (1). The Z^0 production process $e^+p \rightarrow e^+Z^0X$, with a cross section of around 0.3 pb , has been simulated using EPVEC in order to estimate the contribution of $Z^0 \rightarrow l^+l^-$ and $Z^0 \rightarrow \nu\bar{\nu}$ decays to the high- P_T lepton samples considered here.

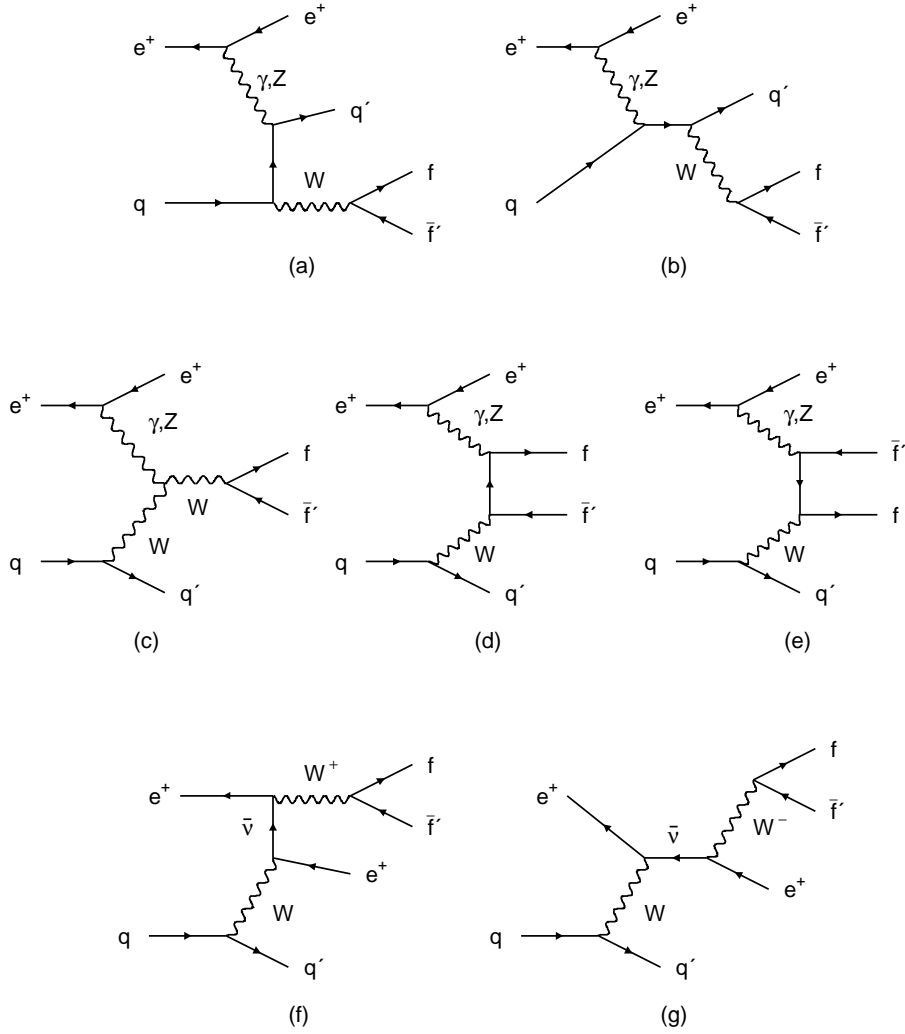


Figure 1: *Leading-order Feynman diagrams for the process $e^+p \rightarrow e^+W^\pm X, W \rightarrow f\bar{f}'$. See text for more details.*

2.2 Cross-Section Uncertainties

The use of different proton and photon parton densities changes the calculated W -production cross section by up to 5% and 10%, respectively. Large uncertainties also result from the choice of hard scale used to evaluate the structure functions. Added in quadrature, the combined effect of these uncertainties leads to an estimated overall uncertainty in the W -production cross section of about 20%.

EPVEC is a leading-order program and includes no QCD radiation. A recent calculation of the cross section for reaction (1) includes a next-to-leading-order (NLO) calculation of

the resolved-photon contribution [7]. The result is 0.97 pb, close to the EPVEC estimate of 0.95 pb. The scale dependence of the NLO cross section is reduced to the 5-10% level, although the structure-function-related uncertainties remain. Changes to the hadronic- P_T spectrum due to higher-order effects, which could be important for some acceptance calculations and for setting coupling limits, are currently unknown.

3 Background Processes

The most important background to W production in the electron decay channel arises from high- Q^2 charged- and neutral-current deep inelastic scattering. These have both been simulated using the event generator DJANGO6 [8], an interface to the Monte Carlo programs HERACLES 4.5 [9] and LEPTO 6.5 [10]. Leading-order QCD and electroweak radiative corrections are included and higher-order QCD effects are simulated via parton cascades using both the parton shower and matrix elements approach of LEPTO and the colour-dipole model ARIADNE [11]. The final hadronisation of the partonic final state is performed with JETSET [12].

Two-photon processes provide an additional source of high- P_T leptons which are a significant background in the muon decay channel. The dominant, Bethe-Heitler, process has been simulated using the event generator LPAIR [13] including both elastic and inelastic production at the proton vertex.

Finally, photoproduction has been simulated with the HERWIG [14] Monte Carlo program, including both resolved and direct photon contributions.

4 The ZEUS Detector

A detailed description of the ZEUS detector can be found elsewhere [15, 16]. The main components used in this analysis were the compensating uranium-scintillator calorimeter (CAL) and the central tracking detector (CTD).

The CAL is divided into three parts, forward (FCAL) covering the polar angle² interval $3^\circ < \theta < 37^\circ$, barrel (BCAL) covering the range $37^\circ < \theta < 129^\circ$ and rear (RCAL) covering the range $129^\circ < \theta < 176^\circ$, as viewed from the nominal interaction point [17]. Each part is divided into towers approximately 20×20 cm in transverse size and segmented longitudinally into an electromagnetic (EMC) section and two hadronic (HAC) sections (one in RCAL). Within the EMC section each tower is further subdivided transversely into four cells (two in RCAL). Each cell is read out by a pair of wavelength shifters and photomultiplier tubes. Calorimeter energy resolutions of $\sigma_E/E = 18\%/\sqrt{E(\text{GeV})}$ for

²The ZEUS coordinate system is right-handed with the Z -axis pointing in the proton beam direction and the horizontal X -axis pointing towards the centre of HERA. The polar angle, θ , is measured with respect to the $+Z$ -axis and the pseudorapidity, η , is related to the polar angle by $\eta = -\ln(\tan(\theta/2))$.

electrons and $\sigma_E/E = 35\%/\sqrt{E(\text{GeV})}$ for hadrons have been measured under test-beam conditions. An instrumented-iron backing calorimeter (BAC) measures energy leakages from the central uranium calorimeter [18].

The CTD is a cylindrical multi-wire drift chamber operating in a 1.43 T solenoidal magnetic field [19]. A momentum measurement, for tracks passing through at least 2 of the 9 radial superlayers, can be made in the polar angle range $15^\circ < \theta < 164^\circ$. The transverse-momentum resolution for full length tracks can be parameterised as $\sigma(P_T)/P_T = 0.0058 P_T \oplus 0.0065 \oplus 0.0014/P_T$, with P_T in GeV.

The luminosity is determined from the rate of high-energy photons produced in the process $ep \rightarrow ep\gamma$ which are measured in a lead-scintillator calorimeter located at $Z = -107$ m [20].

The ZEUS three-level trigger system efficiently selects events with large missing and total transverse energies [16]. Several triggers at each level are used to tag events used for this analysis, with the relevant energy thresholds generally reduced if a good CTD track is present in addition to large calorimeter energies. Algorithms based on tracking and calorimeter timing information reject non- ep backgrounds, consisting mainly of proton beam-gas interactions and cosmic rays.

5 Event Reconstruction and Pre-selection

The calorimeter transverse momentum is defined as :

$$\text{calorimeter } P_T = \sqrt{\left(\sum_i p_{X,i}\right)^2 + \left(\sum_i p_{Y,i}\right)^2}, \quad (2)$$

where $p_{X,i} = E_i \sin \theta_i \cos \phi_i$ and $p_{Y,i} = E_i \sin \theta_i \sin \phi_i$ are calculated using the energies (E_i) of individual calorimeter cells that are above noise thresholds of 80 MeV (EMC) and 140 MeV (HAC). The angles θ_i and ϕ_i are estimated from the geometric cell centres and the event vertex. Note that in $W \rightarrow e\nu$ events, calorimeter P_T as defined above is an estimate of the missing P_T or transverse momentum carried by the neutrino. In muon events, a combination of the calorimeter P_T and the transverse momentum of the muon track measured in the CTD is used to calculate the missing P_T .

Electron (hadron) transverse momenta are defined as sums over those calorimeter cells that are (are not) assigned to the electron candidate cluster. Longitudinal momentum conservation ensures that $E - p_Z$, defined as :

$$E - p_Z = \sum_i E_i (1 - \cos \theta_i),$$

peaks at $2E_e$ for fully contained events, where E_e is the electron beam energy. Smaller values of $E - p_Z$ indicate energy escaping detection, either in the rear beam pipe or in the form of muons or neutrinos.

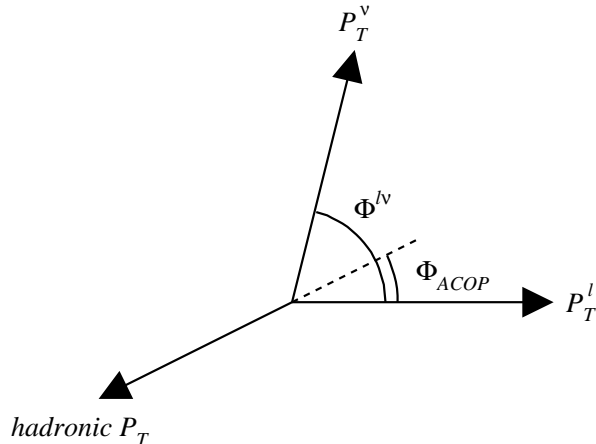


Figure 2: *The definition of the acoplanarity angle, Φ_{ACOP} , and the azimuthal separation of the neutrino and outgoing lepton, $\Phi^{l\nu}$, in the transverse plane. The dashed line balances the hadronic P_T . See text for more details.*

The acoplanarity angle Φ_{ACOP} , illustrated in Fig. 2, is the azimuthal separation of the outgoing lepton and the vector in the $\{X, Y\}$ -plane that balances the hadronic- P_T vector. For well measured neutral-current events the acoplanarity angle is close to zero, while large acoplanarity angles indicate large missing energies. The transverse mass [21] is defined as

$$M_T = \sqrt{2 P_T^l P_T^\nu (1 - \cos \Phi^{l\nu})} ,$$

where P_T^l is the lepton transverse momentum, P_T^ν is the magnitude of the missing P_T and $\Phi^{l\nu}$ is the azimuthal separation of the lepton and missing- P_T vectors, as shown in Fig. 2.

Events that pass the trigger requirements are further required to have a reconstructed calorimeter P_T in excess of 12 GeV. The transverse momentum, calculated excluding the inner ring of calorimeter cells around the forward beam-pipe hole, must be greater than 9 GeV. These offline cuts are more stringent than the corresponding online trigger thresholds in any given year of data taking. Other pre-selection cuts common to both the electron and muon event selections are the requirements that the Z -coordinate of the tracking vertex be reconstructed within 50 cm of the nominal interaction point and have at least one associated track with transverse momentum greater than 0.2 GeV and a polar angle in the range $15^\circ < \theta < 164^\circ$. Cuts on the calorimeter timing and algorithms based on the pattern of tracks in the CTD reject beam-gas, cosmic-ray and halo-muon events.

6 Search for W Production and Decay $W \rightarrow e\nu$

Electron-identification criteria are applied to the pre-selected events and the data are subsequently compared to the Monte Carlo simulation. Final results are presented after

further cuts designed to optimise the sensitivity to the W -production signal.

6.1 Electron Identification

A neural-network-based algorithm to identify electrons, trained on Monte Carlo events and optimised for maximum electron-finding efficiency and electron-hadron separation, selects candidate electromagnetic clusters in the calorimeter [22]. A cut on the electromagnetic-cluster energy of 8 GeV is made, above which the neural network is fully efficient except at the boundaries between the different calorimeter parts. The impact point of the electron at the face of the calorimeter is determined with a resolution of 1 cm using the pulse height information from the pairs of photomultipliers reading out each cell. The distance of closest approach of a matching extrapolated CTD track to the electromagnetic cluster is required to be less than 10 cm, where only tracks with $15^\circ < \theta < 164^\circ$ are considered. The background from fake electrons is reduced by requiring that the energy not associated with the electron in an $\{\eta, \phi\}$ cone of radius 0.8 around the electron direction be less than 4 GeV. Moreover, since most fake electron candidates are misidentified hadrons close to jets, this background is further reduced by requiring that the electron track be separated by at least 0.5 units in $\{\eta, \phi\}$ space from other tracks associated with the event vertex.

6.2 Comparison of Data and Monte Carlo

The data are compared to the expectation from the Monte Carlo simulation in Fig. 3, after requiring that the transverse momentum of the electron, P_T^e , be greater than 5 GeV and the polar angle of the electron measured in the calorimeter, θ_e , be less than 2.0 rad. Neutral-current background events dominate the sample at this stage of the selection, as is evident from the steeply falling missing- P_T spectrum and the concentration of events at small acoplanarity angles. A Jacobian-peak structure is visible in the transverse-mass distribution for the Monte Carlo simulation of the signal events, shown in Fig. 3(f). Figure 3(g) shows the P_T reconstructed in the backing calorimeter and Fig. 3(h) shows the azimuthal separation between the BAC P_T and uranium-calorimeter missing- P_T directions, for events with BAC energy deposits. All distributions show reasonable agreement between the data and Monte Carlo.

6.3 Final Cuts and Results

The neutral-current background is heavily suppressed by requiring the missing P_T to be greater than 20 GeV and the acoplanarity angle to be greater than 0.3 rad, indicated by the arrows in Figs. 3(d) and (e). The latter cut is only applied to events with a hadronic P_T in excess of 4 GeV, for which the acoplanarity angle is well defined. Electrons in the final event sample must, in addition, have $P_T^e > 10$ GeV and $\theta_e < 1.5$ rad. Neutral-current background is further reduced by removing events with energy deposits in the backing

ZEUS 1994-97

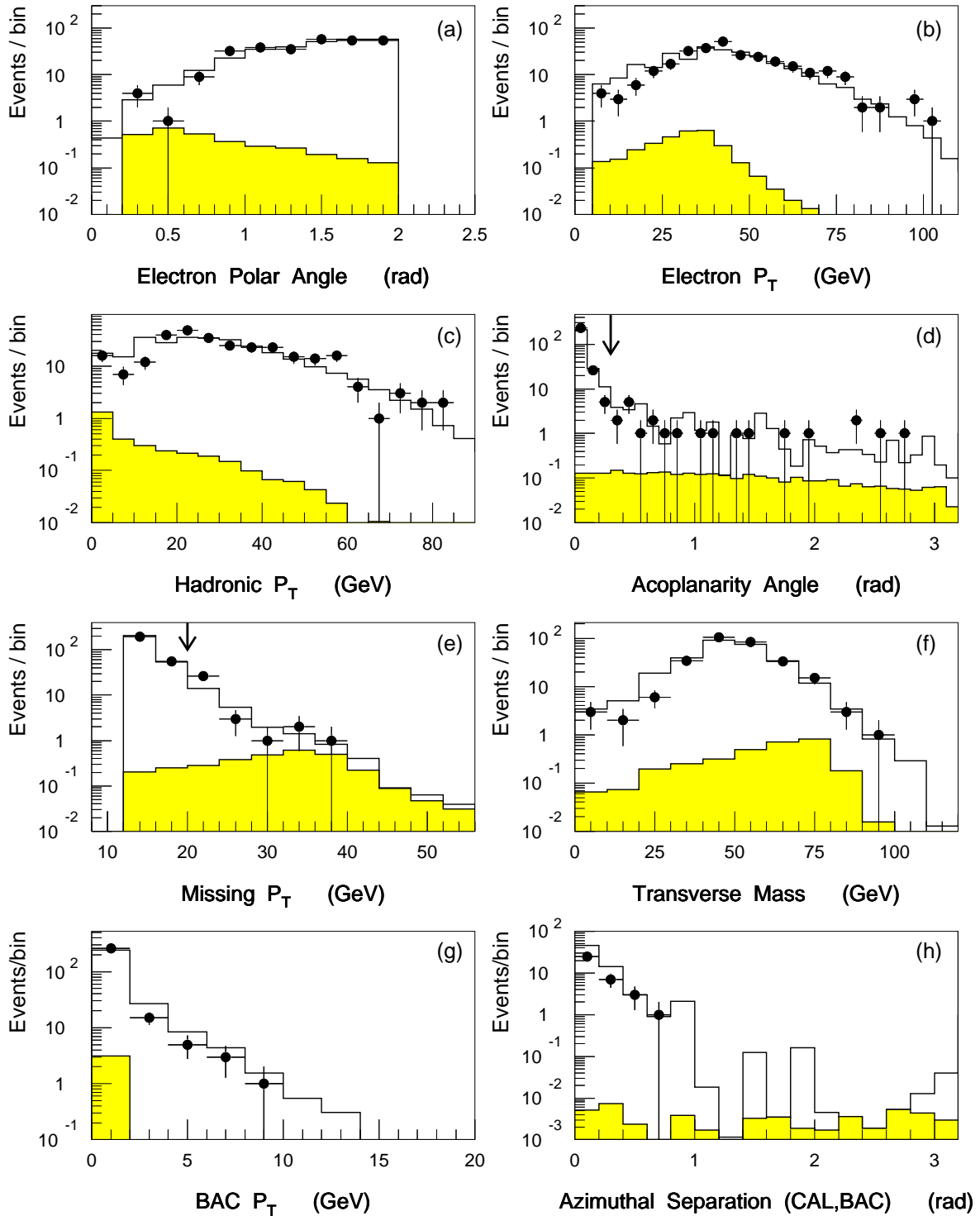


Figure 3: The data (points) compared to the combined luminosity-weighted Monte Carlo expectation (open histograms) for events containing a high- P_T electron in addition to large missing P_T . The W -production component of the Monte Carlo is indicated by the shaded histogram for each distribution. The cuts on the acoplanarity angle and missing P_T used to suppress the neutral-current background are indicated by the arrows in (d) and (e). Only events with BAC energy deposits are plotted in (h).

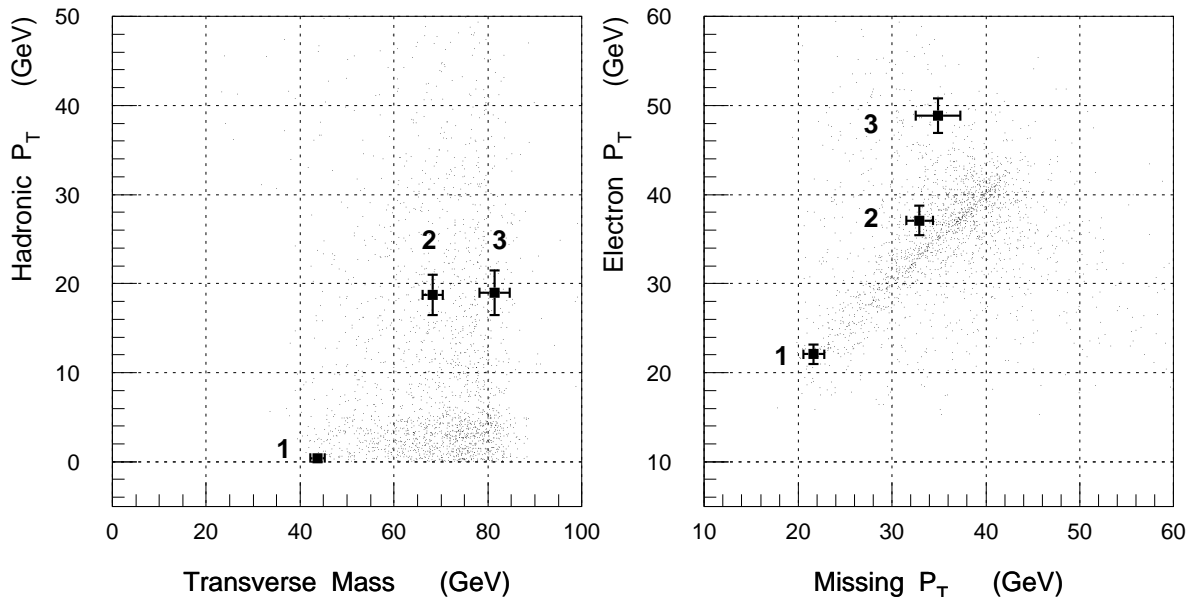


Figure 4: *Characteristic kinematic variables of the three surviving events in the electron sample (square points) and W -production Monte Carlo corresponding to 50 fb^{-1} (dots) after all cuts. All quantities are corrected as described in the text and the errors on the data points are indicated by the error bars. Note that the Monte Carlo simulation is not expected to reproduce accurately the true hadronic- P_T distribution in the region of low hadronic P_T , where W production via resolved photons dominates.*

calorimeter that are closely aligned with the direction of the missing P_T . Finally, requiring that the matching electron track have a transverse momentum greater than 5 GeV, as measured in the CTD, removes most of the remaining fake electrons.

Three data events, all of which have a final-state e^+ , survive these cuts. The properties of these events are given in Table 1 and compared in Fig. 4 to the W -production Monte Carlo with all cuts applied. For these figures and the table, the electron and hadron energies used in calculating the missing P_T and transverse mass have been corrected for the effect of the inactive material between the ep interaction point and the calorimeter. The corrections are typically a few percent for the electron and 10% for the hadron transverse momenta. The momenta of the electrons measured in the CTD agree within errors with the corrected associated calorimeter energies. Given the different cross sections and selection efficiencies for W^+ and W^- production and decay, roughly 60% of signal events are expected to have an e^+ rather than an e^- in the final state, while background events are expected to contain predominantly e^+ candidates. The charge composition of the sample is therefore consistent with expectations. The event in Table 1 with the highest transverse mass is illustrated in Fig. 5. Event 2 has a similar topology while

candidate	1	2	3
electron polar angle	37°	54°	58°
P_T^e (GeV)	22.1 ± 1.1	37.1 ± 1.6	48.8 ± 2.0
matching track P_T (GeV)	$22.3^{+6.8}_{-4.2}$	$35.9^{+13.8}_{-7.8}$	$44.1^{+33.0}_{-13.2}$
track charge	+1 ($> 4\sigma$)	+1 ($> 3\sigma$)	+1 ($> 2\sigma$)
hadronic P_T (GeV)	0.4 ± 0.1	18.7 ± 2.2	19.0 ± 2.5
hadronic $E - p_Z$ (GeV)	0.50	19.4	22.0
missing P_T (GeV)	21.7 ± 1.1	32.9 ± 1.4	34.9 ± 2.4
transverse mass (GeV)	43.7 ± 1.6	68.2 ± 2.2	81.4 ± 3.2

Table 1: *The properties of the three surviving events in the search for W production and decay $W \rightarrow e\nu$. The numbers in parentheses after the track charge indicate the significance of the sign determination.*

event 1 has no visible hadronic jet and consequently a small value for the reconstructed hadronic P_T .

The Monte Carlo expectation after all cuts is 2.1 signal events and 1.1 ± 0.3 background events. The background consists mainly of charged-current DIS, with smaller contributions from Bethe-Heitler di-lepton production and $Z^0 \rightarrow \nu\bar{\nu}$ events in which the beam electron is scattered at small polar angles. Taking into account the efficiency for selecting $W \rightarrow e\nu$ events of 38% and the small extra sensitivity resulting from a $\sim 2\%$ efficiency for selecting $W \rightarrow \tau\nu$ decays, the three events, after subtracting the expected background, correspond to a measured cross section for reaction (1) of :

$$\sigma(e^+p \rightarrow e^+W^\pm X) = 0.9^{+1.0}_{-0.7} \text{ (stat.)} \pm 0.2 \text{ (syst.) pb} .$$

The systematic error is a combination of the uncertainty in the selection efficiency for $W \rightarrow e\nu$ events, the uncertainty in the estimate of the remaining background to W production and decay, and a small contribution from the uncertainty in the total integrated luminosity. The systematic uncertainty in the selection efficiency arises from uncertainties in the electron-finding procedure and the 3% uncertainty in the absolute calorimeter energy scale. The error on the background estimate is a combination of statistical errors and uncertainties due to the choice of model for simulating parton cascades in the DIS Monte Carlo.

From the three observed events, an explicit upper limit on the W -production cross section has been derived, using the background expected from Monte Carlo and applying the

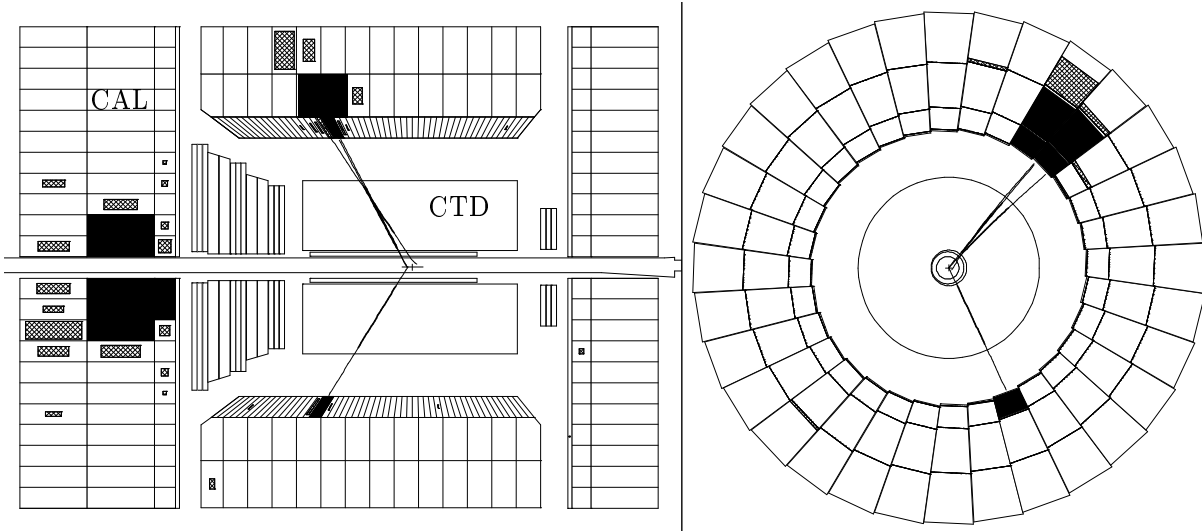


Figure 5: *Event 3 in the final $W \rightarrow e\nu$ data sample, shown in a plane parallel (left) and perpendicular (right) to the beam line. The shaded areas in the calorimeter indicate energy deposits. An electron is visible in the lower half of the segmented uranium calorimeter, acoplanar with a jet of hadrons visible in the upper half. The transverse mass for the event is 81.4 ± 3.2 GeV.*

method described in [23] :

$$\sigma(e^+p \rightarrow e^+W^\pm X) < 3.3 \text{ pb at 95\% C.L.}$$

The selection efficiency in the electron channel depends little on the recoiling hadronic P_T . This implies that the upper limit given above is insensitive to uncertainties in the underlying hadronic- P_T distribution arising from higher-order effects or anomalous $WW\gamma$ couplings.

7 Search for W Production and Decay $W \rightarrow \mu\nu$

The search for reaction (1) with the subsequent decay $W \rightarrow \mu\nu$ begins with the same sample of events with a large calorimeter missing P_T used in the electron analysis (see Section 5). However, since a high-energy muon leaves only a small energy deposit in the calorimeter, this selection necessarily restricts the acceptance to W -production events with large hadronic transverse momenta.

7.1 Muon Identification

The energy deposited by minimum-ionising particles (MIP's) can be distributed across several calorimeter clusters. Therefore neighbouring clusters are grouped together into

larger scale objects which, providing they pass topological and energy cuts, are called calorimeter MIP's. In this analysis, a muon candidate is simply a calorimeter MIP that matches an extrapolated CTD track within 20 cm, where only tracks in the polar angle range $15^\circ < \theta < 164^\circ$ are considered. The muon transverse momentum, P_T^μ , and direction, including the polar angle, θ_μ , are obtained from the matching CTD track. The same energy- and track-isolation requirements made in the electron analysis are also applied here to the muon candidate.

7.2 Comparison of Data and Monte Carlo

The data and Monte Carlo predictions are compared in Fig. 6, after requiring $P_T^\mu > 5$ GeV and $\theta_\mu < 2.0$ rad. Events with more than one muon candidate having $P_T^\mu > 2$ GeV have been removed. Fig. 6(d) shows the missing transverse momentum, calculated by combining the muon and calorimeter P_T 's in the transverse plane after subtracting the muon's contribution to the latter. In each case the distribution of events is similar to that expected from the Monte Carlo simulation of the background, which is dominated by Bethe-Heitler di-muon production.

7.3 Final Cuts and Results

The final stage in the selection of $W \rightarrow \mu\nu$ events requires the missing transverse momentum to be greater than 15 GeV. No data event survives this final cut, shown in Fig. 6(d), to be compared with an expected 0.76 events from W production and 0.65 ± 0.22 from background. The latter is dominated by charged-current DIS and Bethe-Heitler $\mu^+\mu^-$ production. The efficiency for selecting $W \rightarrow \mu\nu$ events is 13%, lower than the corresponding efficiency in the electron channel due to the soft hadronic- P_T spectrum expected for reaction (1). The resulting 95% C.L. upper limit on the cross section for this reaction is therefore weaker, at 3.7 pb. Note that the value for the efficiency in the muon channel, calculated here using EPVEC, is much more sensitive to assumptions about the hadronic- P_T distribution than the corresponding efficiency in the electron channel.

8 W Production at Large Hadronic P_T

The final electron and muon samples described in Sections 6.3 and 7.3, respectively, are combined and events which have large hadronic P_T are selected. The number of events with a corrected hadronic P_T above specified values is shown in Table 2, along with the number of W -production and background events expected from Monte Carlo. The efficiencies listed in the table have been calculated for the subset of W -production events that have a true hadronic P_T above the given value. They are averaged over all decay channels, thereby including a small contribution from $W \rightarrow \tau\nu$ decays. The resulting 95% C.L. upper limits on the cross section for the reaction $e^+p \rightarrow e^+W^\pm X$ at large

ZEUS 1994-97

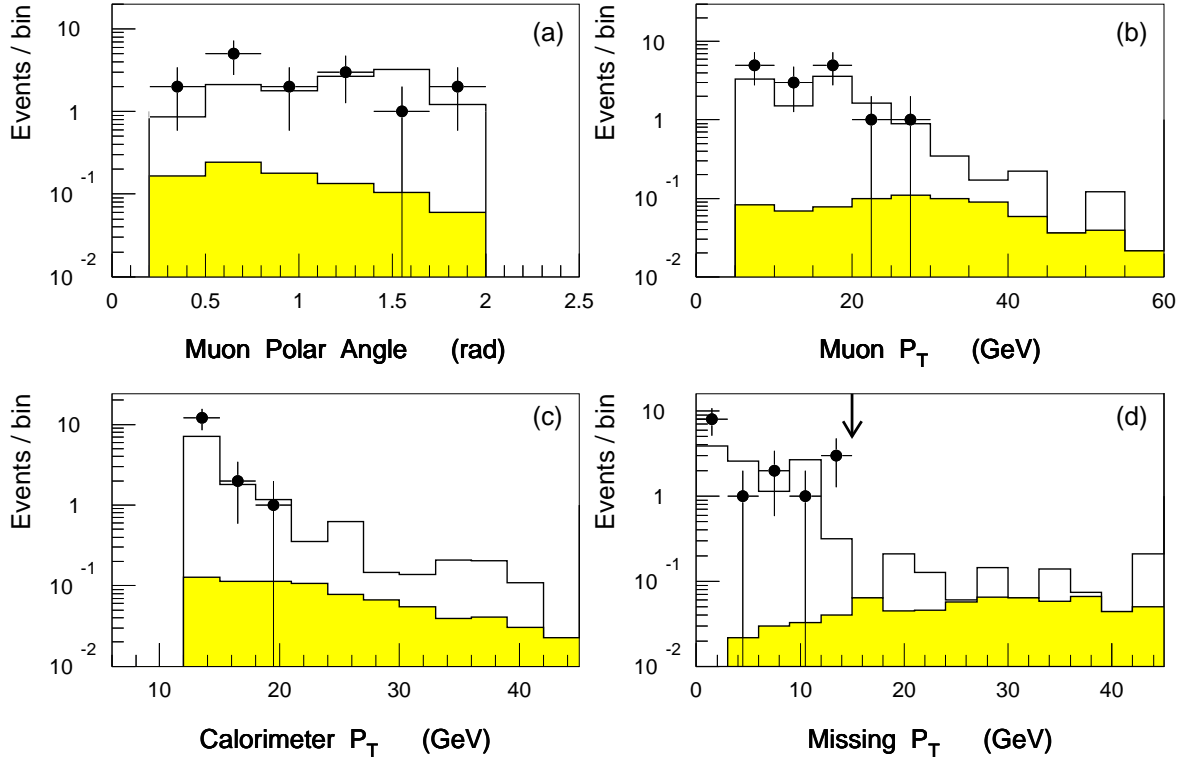


Figure 6: *The data (points) compared to the combined luminosity-weighted Monte Carlo expectation (open histogram) for events containing a high- P_T muon in addition to large calorimeter P_T . The W -production component of the Monte Carlo is given in each distribution by the shaded histogram. The final cut on the missing P_T is indicated by the arrow in (d).*

hadronic P_T are also given in the table. Note that the selection efficiency in the muon channel is small for low hadronic P_T , reaching a plateau comparable to the efficiency in the electron channel at around 20 GeV. Cross-section limits for cuts on the hadronic P_T at or above this value are insensitive to the underlying hadronic- P_T distribution.

The limits given in Table 2 can be used to constrain various any new physics processes which produce events with a W boson and large hadronic P_T . Such model-dependent analyses are outside of the scope of this paper. It is nevertheless useful to parameterise such effects in terms of anomalous $WW\gamma$ couplings, which give rise to a harder distribution of the transverse momentum of the W than expected in the Standard Model. The most general effective Lagrangian that is consistent with Lorentz invariance, CP conservation and electromagnetic gauge invariance, has two free couplings at the $WW\gamma$ vertex that are conventionally labelled κ and λ [1, 24]. In the Standard Model they take the values

hadronic P_T	data	Standard Model Monte Carlo			95% C.L. cross section upper limit
		W	background	W efficiency	
> 15 GeV	2	1.4	0.62 ± 0.20	10%	1.2 pb
> 20 GeV	0	1.2	0.52 ± 0.18	11%	0.58 pb
> 25 GeV	0	0.89	0.49 ± 0.18	11%	0.56 pb

Table 2: *The results of a search for events with large hadronic P_T in the combined electron and muon samples. The number of observed events is compared to the Monte Carlo expectation for Standard Model W production and background, after a cut on the corrected hadronic P_T . Selection efficiencies are averaged over all W decay channels and the upper limits are on the cross section for reaction (1) above the indicated hadronic P_T .*

$\kappa = 1$ and $\lambda = 0$; deviations are parameterised in terms of the anomalous couplings $\Delta\kappa = \kappa - 1$ and λ . The dependence of the total W -production cross section on these anomalous couplings is calculated using EPVEC. For example, the upper limit of 0.58 pb for hadronic $P_T > 20$ GeV corresponds to the following 95% C.L. limits on $\Delta\kappa$ and λ :

$$\begin{aligned}
-4.7 < \Delta\kappa < 1.5 \quad (\lambda = 0) , \\
-3.2 < \lambda < 3.2 \quad (\Delta\kappa = 0) .
\end{aligned}$$

These limits on anomalous $WW\gamma$ couplings are insensitive to the assumed couplings at the WWZ vertex due to the suppression by the propagator mass. They are however significantly larger than the limits derived from analyses at the Tevatron [25] and LEP2 [26].

9 Isolated-Track Search

The H1 collaboration has recently reported the observation of six events containing an isolated high- P_T lepton and large missing P_T in 36.5 pb^{-1} of e^+p data [4]. The H1 search required isolated tracks with $P_T > 10$ GeV and a calorimeter P_T exceeding 25 GeV. Five of the events contain muons, which may be compared to the 0.5 W events and 0.25 other events (mainly $\gamma\gamma \rightarrow \mu^+\mu^-$) expected.

Although the ZEUS data presented above are in good agreement with Standard Model expectations, a separate search has been performed for isolated high- P_T tracks in events with a large missing P_T , applying cuts similar to those used by H1. Because of the typical 10% difference between observed and corrected hadronic- P_T values, all events that have an uncorrected calorimeter P_T greater than 20 GeV are selected. In addition, the events are required to contain at least one jet with $E_T > 5$ GeV, an electromagnetic fraction less than 0.9 and an angular size greater than 0.1 rad. Events with a neutral-current topology

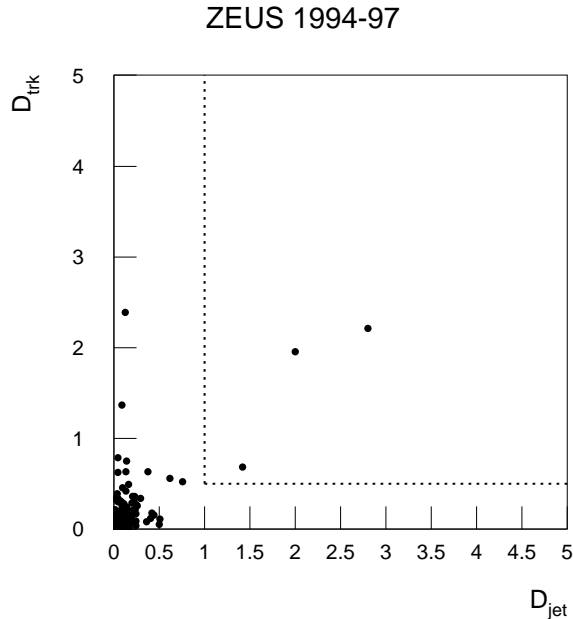


Figure 7: *The jet and track $\{\eta, \phi\}$ isolation of high- P_T tracks in events with large missing P_T . The cuts used to select the tracks are described in the text. The dotted lines define the region of interest.*

that have an acoplanarity angle less than 0.2 rad are excluded. The high- P_T track must pass through at least 3 radial superlayers of the CTD (corresponding to $\theta \gtrsim 0.3$ rad) and have $\theta < 2.0$ rad. The isolation variables D_{jet} and D_{trk} are defined for a given track as the $\{\eta, \phi\}$ separation of that track from the nearest jet and the nearest neighbouring track in the event, respectively. All tracks with $P_T > 10$ GeV in the selected events are plotted in the $\{D_{\text{trk}}, D_{\text{jet}}\}$ plane in Fig. 7. The 3 tracks selected with $D_{\text{trk}} > 0.5$ and $D_{\text{jet}} > 1.0$ agree well with the expectation of 5.7 ± 0.8 tracks from combined Monte Carlo sources. All three isolated tracks are positively charged and are identified as electrons using the algorithm and criteria described above. This is consistent with the 3.5 ± 0.7 (2.0 ± 0.4) electron type (muon type) events expected from Monte Carlo, of which 0.9 (0.4) are from W production. Two of the isolated tracks correspond to events 2 and 3 of Table 1. The third track is found in an event with neutral-current topology in which there is evidence of a large energy leakage into the backing calorimeter. There is therefore no evidence of an excess of isolated high- P_T tracks, whether identified as leptons or not, in the 1994 – 1997 ZEUS data.

10 Conclusions

A search for the decay $W \rightarrow e\nu$ in e^+p collisions at a centre-of-mass energy of 300 GeV yields three candidate events, of which 1.1 ± 0.3 are estimated to arise from sources other

than W production. This results in an estimate of the cross section for the process $e^+p \rightarrow e^+W^\pm X$ of $0.9_{-0.7}^{+1.0} \pm 0.2$ pb, consistent with the Standard Model prediction. The corresponding 95% C.L. upper limit on the cross section of 3.3 pb is insensitive to uncertainties in the underlying hadronic- P_T distribution. A search for the decay $W \rightarrow \mu\nu$ yields no candidate event, also consistent with Standard Model expectations. Events with large hadronic P_T in the combined electron plus muon sample have been used to set 95% C.L. upper limits on the cross section for W production, for example 0.58 pb for hadronic P_T greater than 20 GeV.

A number of events with large missing P_T and an isolated high- P_T lepton, in excess of Standard Model expectations, has been reported by the H1 collaboration. The search presented in this paper, with similar cuts and sensitivity, has revealed no such excess.

Acknowledgements

This work would not have been possible without the dedicated efforts of the HERA machine group and the DESY computing staff. We would also like to thank the DESY directorate for their strong support and encouragement throughout. The design, construction and installation of the ZEUS detector would not have been possible without the hard work of many people who are not listed as authors. In addition, it is a pleasure to thank U. Baur, D. Zeppenfeld and M. Spira for providing their calculations and for many fruitful discussions.

References

- [1] U. Baur and D. Zeppenfeld, *Nucl. Phys. B* **325** (1989) 253.
- [2] U. Baur, J.A.M. Vermaseren and D. Zeppenfeld, *Nucl. Phys. B* **375** (1992) 3.
- [3] M.N. Dubinin and H.S. Song, *Phys. Rev. D* **57** (1998) 2927.
- [4] H1 Collab., C. Adloff *et al.*, *Eur. Phys. J. C* **5** (1998) 575.
- [5] A.D. Martin, W.J. Stirling and R.G. Roberts, *Phys. Lett. B* **354** (1995) 155.
- [6] M. Glück, E. Reya and A. Vogt, *Phys. Rev. D* **45** (1992) 3986.
- [7] P. Nason, R. Rückl and M. Spira, hep-ph/9902296, to appear in Proc. of the “3rd UK Phenomenology Workshop on HERA Physics”, Durham, 1998; M. Spira, private communication.
- [8] K. Charchuła, G.A. Schuler and H. Spiesberger, *Comp. Phys. Commun.* **81** (1994) 381.

- [9] A. Kwiatkowski, H. Spiesberger and H.-J. Möhring, *Comp. Phys. Commun.* **69** (1992) 155.
- [10] G. Ingelman, A. Edin and J. Rathsman, *Comp. Phys. Commun.* **101** (1997) 108.
- [11] L. Lönnblad, *Comp. Phys. Commun.* **71** (1992) 15.
- [12] T. Sjöstrand, *Comp. Phys. Commun.* **39** (1986) 347;
T. Sjöstrand and M. Bengtsson, *Comp. Phys. Commun.* **43** (1987) 367;
T. Sjöstrand, *Comp. Phys. Commun.* **82** (1994) 74.
- [13] J.A.M. Vermaseren, *Nucl. Phys. B* **229** (1983) 347;
S.P. Baranov *et al.*, in Proc. of the Workshop “Physics at HERA”, vol. 3, Eds. W. Buchmüller and G. Ingelman, DESY (1991), 1478.
- [14] G. Marchesini *et al.*, *Comp. Phys. Commun.* **67** (1992) 465.
- [15] ZEUS Collab., M. Derrick *et al.*, *Phys. Lett. B* **293** (1992) 465.
- [16] ZEUS Collab., “The ZEUS Detector”, Status Report 1993, DESY(1993).
- [17] M. Derrick *et al.*, *Nucl. Instrum. Methods A* **309** (1991) 77;
A. Andresen *et al.*, *Nucl. Instrum. Methods A* **309** (1991) 101;
A. Caldwell *et al.*, *Nucl. Instrum. Methods A* **321** (1992) 356;
A. Bernstein *et al.*, *Nucl. Instrum. Methods A* **336** (1993) 23.
- [18] H. Abramowicz *et al.*, *Nucl. Instrum. Methods A* **313** (1992) 126.
- [19] N. Harnew *et al.*, *Nucl. Instrum. Methods A* **279** (1989) 290;
B. Foster *et al.*, *Nucl. Phys. B* (Proc. Suppl.) **32** (1993) 181;
B. Foster *et al.*, *Nucl. Instrum. Methods A* **338** (1994) 254.
- [20] J. Andrusków *et al.*, DESY 92-066 (1992);
ZEUS Collab., M. Derrick *et al.*, *Z. Phys. C* **63** (1994) 391.
- [21] UA1 Collab., G. Arnison *et al.*, *Phys. Lett. B* **122** (1983) 103.
- [22] H. Abramowicz, A. Caldwell and R. Sinkus, *Nucl. Instrum. Methods A* **365** (1995) 508.
- [23] L. Montanet *et al.* (Particle Data Group), *Phys. Rev. D* **54** (1996) 1.
- [24] K. Hagiwara, K. Hikasa, R.D. Peccei and D. Zeppenfeld, *Nucl. Phys. B* **282** (1987) 253.
- [25] DØ Collab., S. Abachi *et al.*, *Phys. Rev. Lett.* **78** (1997) 3634.
- [26] L3 Collab., M. Acciarri *et al.*, *Phys. Lett. B* **436** (1998) 417.